Biophysical Journal
Article

Biophysical Society

Dynamic and Irregular Distribution of RyR2 Clusters in the Periphery of Live Ventricular Myocytes

Florian Hiess,[1] Pascal Detampel,[2] Carme Nolla-Colomer,[3] Alex Vallmitjana,[3] Anutosh Ganguly,[4] Matthias Amrein,[5] Henk E. D. J. ter Keurs,[1] Raul Benítez,[3] Leif Hove-Madsen,[6] and S. R. Wayne Chen[1,*]

[1]Libin Cardiovascular Institute of Alberta, Department of Physiology and Pharmacology, University of Calgary, Calgary, Alberta, Canada; [2]Department of Pharmaceutical Sciences, University of Basel, Basel, Switzerland; [3]Automatic Control Department, Universitat Politècnica de Catalunya-Barcelona Tech, Barcelona, Spain; [4]Department of Microbiology, Immunology and Infectious Diseases and [5]Department of Biology and Anatomy, University of Calgary, Calgary, Alberta, Canada; and [6]Biomedical Research Institute Barcelona CSIC-IIBB, Sant Pau, Hospital de Sant Pau, Barcelona, Spain

ABSTRACT Cardiac ryanodine receptors (RyR2s) are Ca^{2+} release channels clustering in the sarcoplasmic reticulum membrane. These clusters are believed to be the elementary units of Ca^{2+} release. The distribution of these Ca^{2+} release units plays a critical role in determining the spatio-temporal profile and stability of sarcoplasmic reticulum Ca^{2+} release. RyR2 clusters located in the interior of cardiomyocytes are arranged in highly ordered arrays. However, little is known about the distribution and function of RyR2 clusters in the periphery of cardiomyocytes. Here, we used a knock-in mouse model expressing a green fluorescence protein (GFP)-tagged RyR2 to localize RyR2 clusters in live ventricular myocytes by virtue of their GFP fluorescence. Confocal imaging and total internal reflection fluorescence microscopy was employed to determine and compare the distribution of GFP-RyR2 in the interior and periphery of isolated live ventricular myocytes and in intact hearts. We found tightly ordered arrays of GFP-RyR2 clusters in the interior, as previously described. In contrast, irregular distribution of GFP-RyR2 clusters was observed in the periphery. Time-lapse total internal reflection fluorescence imaging revealed dynamic movements of GFP-RyR2 clusters in the periphery, which were affected by external Ca^{2+} and RyR2 activator (caffeine) and inhibitor (tetracaine), but little detectable movement of GFP-RyR2 clusters in the interior. Furthermore, simultaneous Ca^{2+}- and GFP-imaging demonstrated that peripheral RyR2 clusters with an irregular distribution pattern are functional with a Ca^{2+} release profile similar to that in the interior. These results indicate that the distribution of RyR2 clusters in the periphery of live ventricular myocytes is irregular and dynamic, which is different from that of RyR2 clusters in the interior.

INTRODUCTION

Cardiac ryanodine receptors (RyR2s) are intracellular Ca^{2+} release channels. They reside in the sarcoplasmic reticulum (SR) membrane of myocytes and are crucial for excitation-contraction coupling (ECC) (1,2). In this process, membrane depolarization leads to a small Ca^{2+} influx into the cytosol via the voltage-dependent L-type Ca^{2+} channel. This subsequently triggers a more substantial Ca^{2+} release from the SR via RyR2s, leading to muscle contraction (1,2). This RyR2-mediated Ca^{2+} amplification is known as "Ca^{2+}-induced Ca^{2+} release" (CICR). As a positive feedback mechanism, CICR has the inherent potential for unwanted self-regenerative Ca^{2+} release. However, despite potential regeneration, cardiac ECC is graded and tightly controlled (3–9). The distribution and function of RyR2s are believed to be crucial for graded CICR during ECC. Stern (7) showed that close proximity of voltage-dependent L-type Ca^{2+} channels and RyR2s permit graded coupling between Ca^{2+} influx and Ca^{2+} release.

RyR2s themselves have been found to arrange into clusters, which are thought to be the elementary functional units (5–7,10–14). Ca^{2+} release from one of these elementary units has been termed "Ca^{2+} spark" (3,12,15–17). Global Ca^{2+} events are the spatiotemporal summation of Ca^{2+} sparks (17). Hence, graded SR Ca^{2+} release is explicable via the recruitment of variable numbers of RyR2 Ca^{2+} release units (3,12,15,16,18,19). The effectiveness of such recruitment would depend on the distribution of the RyR2 Ca^{2+} release units or RyR2 clusters. The spacing of these RyR2 clusters has also been suggested to be an important determinant of the initiation of spontaneous propagating Ca^{2+} events (20). Thus, understanding the distribution of RyR2 clusters is important for elucidating the fundamental mechanism of CICR.

Submitted July 7, 2017, and accepted for publication November 3, 2017.

*Correspondence: swchen@ucalgary.ca

Editor: Eric Sobie.

https://doi.org/10.1016/j.bpj.2017.11.026

The distribution of RyR2s has been extensively studied (14,21–30). Tightly organized arrays of RyR2 clusters with single transverse rows have been found in the interior of ventricular myocytes. In contrast, different patterns of RyR2 distribution were observed in the peripheral region. On the one hand, 3D confocal imaging studies showed an irregular pattern of distribution of RyR2 clusters in the outermost optical confocal *z*-planes (26–28). On the other hand, total internal reflection fluorescence (TIRF) imaging (29,30) reported a double-row pattern of distribution of RyR2 clusters near the sarcolemmal membrane. The exact reason for this discrepancy is unclear. Confocal imaging collects light from optical segments >500 nm (31,32). Hence, disordered distribution observed by confocal imaging could be due to the capture of signals from multiple layers near, but not only from, the periphery. In contrast, TIRF imaging is used to capture signals close to the cell surface (31,32). Thus, one would propose that double-rows of RyR2 clusters observed using TIRF may reflect RyR2 distribution in the periphery.

Nearly all studies of the distribution of RyR2 clusters have been carried out in fixed and permeabilized cells/tissues using RyR2 antibody immunostaining (14,21–30,33,34). Hence, sample preparation (fixation and permeabilization) required for immunostaining may change cellular structures, besides rendering the cells/tissues nonfunctional (35). Furthermore, the specificity and accessibility of the antibodies may be of concern under some experimental conditions. Moreover, it appears that there are three patterns of distribution of RyR2 clusters located near the sarcolemmal membrane of cardiomyocytes: 1) irregular/disordered, 2) double rows, and 3) single rows. Although, it is well known that there are functional RyR2 clusters located near the membrane (36–38), whether all these RyR2 clusters with different patterns of distribution are activated by Ca^{2+} influx through the L-type Ca^{2+} channel or function similarly to those in the interior is unclear. These issues make the need to study the in situ distribution and function of RyR2 clusters in living cells without tissue fixation and permeabilization for the use of antibodies clearly evident.

We recently generated a knock-in mouse model expressing a green fluorescent protein (GFP)-tagged RyR2 (39). This model provides a tool to study the distribution and function of RyR2 clusters in intact live cells without the need for immunostaining, thus avoiding the aforementioned concerns. In a previous study (39), we revealed highly organized arrays of GFP-RyR2 clusters that correlate with the Ca^{2+} release sites in the interior of ventricular myocytes. In this study, we employed 3D confocal imaging and TIRF microscopy to determine and compare the distribution of GFP-RyR2 in the interior and periphery in isolated ventricular myocytes and in intact hearts from the GFP-RyR2 mice. We confirmed the existence of tightly ordered arrays of GFP-RyR2 clusters in the cell interior. In contrast, an irregular pattern of distribution of GFP-RyR2 clusters was observed in the periphery using both imaging techniques. Moreover, unlike interior RyR2 clusters that showed little detectable movement, irregularly distributed peripheral RyR2 clusters displayed dynamic movements that are modulated by RyR2 modulators. Furthermore, we found that peripheral RyR2 form clusters with an irregular distribution pattern function with a Ca^{2+} release profile similar to that of RyR2 clusters in the interior. These observations provide, to our knowledge, novel insights into the distribution and function of RyR2 clusters in the periphery of living cardiomyocytes.

MATERIALS AND METHODS

Animal studies

All animal studies were approved by the Institutional Animal Care and Use Committees at the University of Calgary and were performed in accordance with US National Institutes of Health guidelines. Adult knock-in mice expressing a GFP-tagged RyR2 (39) and wild-type control littermates (8–16 weeks of age) of both sexes were used.

Isolation of intact hearts

A Langendorff apparatus (40) was employed to perfuse excised hearts from GFP-RyR2 knock-in mice with Krebs-Ringers-HEPES (KRH) buffer (NaCl, 125 mM; KCl, 12.5 mM; HEPES, 25 mM; glucose, 6 mM; $MgCl_2$, 1.2 mM; taurine, 20 mM; 2,3-butandion-monoxim, 20 mM; albumin, 5 mg/mL; $CaCl_2$, 0–1 mM; pH 7.4; oxygenated with 95% O_2 and 5% CO_2) at room temperature. Hearts were then placed onto a recording chamber for 3D confocal live cell imaging of GFP fluorescence signals in epicardial ventricular myocytes.

Single mouse ventricular myocyte preparation for confocal GFP-RyR2 imaging

Single ventricular myocytes were isolated from GFP-RyR2 knock-in mouse hearts using collagenase type II (Worthington Biochem, Lakewood, NJ) and protease digestion. Isolated cells were placed onto laminin-coated glass coverslips in the presence of KRH buffer. After up to 2 h of settling, unattached myocytes were gently removed via KRH buffer exchange and remaining myocytes transferred onto a recording chamber. Cell integrity was tested via pacing at 2 Hz. Only cardiomyocytes that followed electrical pacing were selected for subsequent 3D confocal live cell imaging of GFP-RyR2, as previously described (39).

3D confocal live cell imaging

Confocal (*xy* galvano/resonant) imaging was performed with an inverted A1R, or A1Rplus microscope system (Nikon, Mississauga, ON, Canada) equipped with a Plan-Apochromat 60×/1.2-NA water immersion objective, or Plan-Apochromat 60×/1.27-NA oil immersion objective and selective excitation and emission filters. 3D confocal z-stacks of GFP-RyR2 (Ex/Em 488/510 nm) were acquired in 0.2–0.3 μm z-increments from a region of interest with a vertical/axial thickness of 25–40 μm. All imaging of live cells and tissue was performed no longer than 8 h after their isolation.

Confocal single-cell Ca^{2+} imaging in mouse ventricular myocytes

Ventricular myocytes isolated from GFP-RyR2 mice were loaded with Rhod-2 AM Ca^{2+} indicator (2.5–5 μM; Invitrogen, Waltham, MA) in

KRH buffer for 20 min at room temperature (40). After 20 min deesterification of Rhod-2 AM, the cells were washed, transferred onto laminin-coated cover glasses, and permitted to adhere for up to 2 h. The myocytes were then placed in a recording chamber and exposed to KRH solution containing 2–3 mM free Ca^{2+} at which spontaneous Ca^{2+} release events could be detected.

High-speed confocal *xy* resonant imaging was employed to simultaneously record individual Ca^{2+} release events and GFP-RyR2 fluorescence signals at interior and outermost peripheral xy planes within the same cell. Excitation light was provided by argon (488 nm) and diode (561 nm) lasers to detect GFP-RyR2 (Ex/Em 488/510 nm) and Rhod-2 AM Ca^{2+} indicator signals (Ex/Em 550/580 nm). Image series of Ca^{2+} release events were acquired in 25.5 μm optical sections at a sampling rate of 50–60 frames per second (FPS).

GFP-RyR2 cluster imaging in ventricular myocytes using a TIRF microscope

Isolated ventricular myocytes from GFP-RyR2 mice and wild-type littermates were transferred onto 35 mm glass-bottomed microdishes with or without laminin-coating (Minitube; Ibidi, Fitchburg, WI). Cell adhesion was permitted for up to 2 h in KRH buffer (0.5–1 mM Ca^{2+}), before staging the dishes onto the microscope. Data were acquired with an inverted ELYRA LSM780 microscope (Zeiss, North York, ON, Canada) equipped with an α-Plan-Apochromat 100×/1.46-NA oil immersion objective and excitation and emission filters. Excitation light was provided by an HR Diode 488–100 Laser (488 nm; Zeiss) to detect GFP. Images of the periphery (TIRF mirror angle >64°) and the interior (angle 0) were acquired from the same cell. Layers in between were recorded in stacks with 0.25–0.3 μm *z*-steps (mirror angle 59–62°) with highly inclined and laminated optical sheet (HILO) illumination (35). Whole image intensity profiles for Fourier transforms were obtained with the software Fiji (ImageJ; National Institutes of Health, Bethesda, MD). The intensity profiles were Gaussian-fitted and relative intensity was used for pattern analysis. Time-lapse series were recorded at rates of 1–6 frames per minute for at least 12 min with exposure times of <100 ms per image. The TrackMate (41) ImageJ plugin was used for advanced cluster dynamic analysis.

Ca^{2+} imaging in live GFP-RyR2 expressing cells via a TIRF microscope

Ventricular myocytes isolated from GFP-RyR2 mice were loaded with Fluo-4 AM Ca^{2+} indicator (2.5–5 μM; Invitrogen) plus 0.02% Pluronic F-127 in KRH buffer for 20 min at room temperature. The cells were then washed, and transferred onto 35 mm glass-bottomed microdishes (Minitube; Ibidi). Cell adhesion was permitted for up to 2 h. Spontaneous Ca^{2+} release events were recorded in KRH solution containing 2–3 mM free Ca^{2+}. Time series were acquired with the same TIRF microscope as described above. Excitation light was provided by an HR Diode488-100 laser (488 nm; Zeiss) to detect GFP and simultaneously Fluo-4 Ca^{2+} indicator signals (maximum emission of 506 nm). Images of the periphery and interior of the same cell were obtained. Ca^{2+} dynamics were recorded at 50–60 FPS in multiples of 10 s.

Computational image analysis

Basic image processing of fluorescence signals was performed using the softwares NIS Elements AR 4.13 (Nikon); ZEN Black (Zeiss), and Fiji (ImageJ; National Institutes of Health). Spark detection and characterization system was implemented and performed using the software MATLAB (The MathWorks, Natick, MA).

Automated spark detection and analysis

GFP-RyR2 cluster signals were revealed via average projection from temporal fluorescence image sequences. The brightest GFP-RyR2 cluster sites from each cell were determined semiautomatically after application of an intensity threshold.

Ca^{2+} release images were partitioned using a regular square lattice of size 0.5 μm. In each image of a sequence, the mean fluorescence value was extracted for each grid site to obtain a temporal fluorescence signal for each grid site. Ca^{2+} indicator fluorescence signals (f) corresponding to grid sites that coincided with GFP-RyR2 clusters were used for subsequent analysis. Signal at each site was normalized using the baseline value (f_0) defined as the lower 1% of the fluorescence signal. The continuous wavelet transform was calculated using a $Gauss^2$ wavelet family function, with two scales—one corresponding to short spark-like events (~150 ms) and one associated with long events (~450 ms). Ca^{2+} release event candidates were detected by wavelet thresholding using two sets of heuristic threshold values specific to confocal and TIRF microscopy images.

For this study, only nonpropagating spark-like release events were considered. Thus, events that appeared in both temporal scales and events in the longer temporal scale were discarded. Such events were assumed to correspond to propagating Ca^{2+} release (e.g., miniwaves and waves). For each of them, the following features were determined: absolute peak amplitude, local baseline, amplitude relative to the local baseline, rate of rise, time to peak, full duration at half-maximum, and exponential decay time. This set of features was used to further filter events satisfying preestablished criteria to exclude false positives.

Statistical analysis

All values shown are mean ± SE unless indicated otherwise. To test for differences between groups, we used unpaired Student's t-tests (two-tailed); p values < 0.05 were considered to be statistically significant.

RESULTS

Confocal imaging of interior and peripheral distribution of RyR2 clusters

To study the distribution of RyR2 in different subcellular regions of live ventricular myocytes, we employed our recently generated knock-in mouse model expressing a GFP-tagged RyR2 (39). Using 3D confocal imaging, we detected GFP fluorescence in ventricular myocytes isolated from adult GFP-RyR2 mouse hearts. As shown in Fig. 1 *Aa*, GFP-RyR2s in the interior were organized as arrays of highly ordered clusters. In contrast, imaging focusing near the periphery showed irregular distribution and appearance of RyR2 clusters (Fig. 1 *Ab*). To exclude the possibility that the irregular distribution of RyR2 clusters in the periphery was artificially introduced by cell isolation, we imaged intact hearts from GFP-RyR2 mice. As shown in Fig. 1 *Ba*, optical confocal z-stack planes of the left ventricle showed highly organized arrangements of GFP-RyR2 clusters in the cell interior. In contrast, the distribution of GFP-RyR2 clusters in the periphery of the same area was disordered (Fig. 1 *Bb*). These data indicate that the observation of different distribution patterns of GFP-RyR2 clusters in the interior and periphery was not the result of cell isolation. Thus, RyR2 clusters are organized in a highly ordered

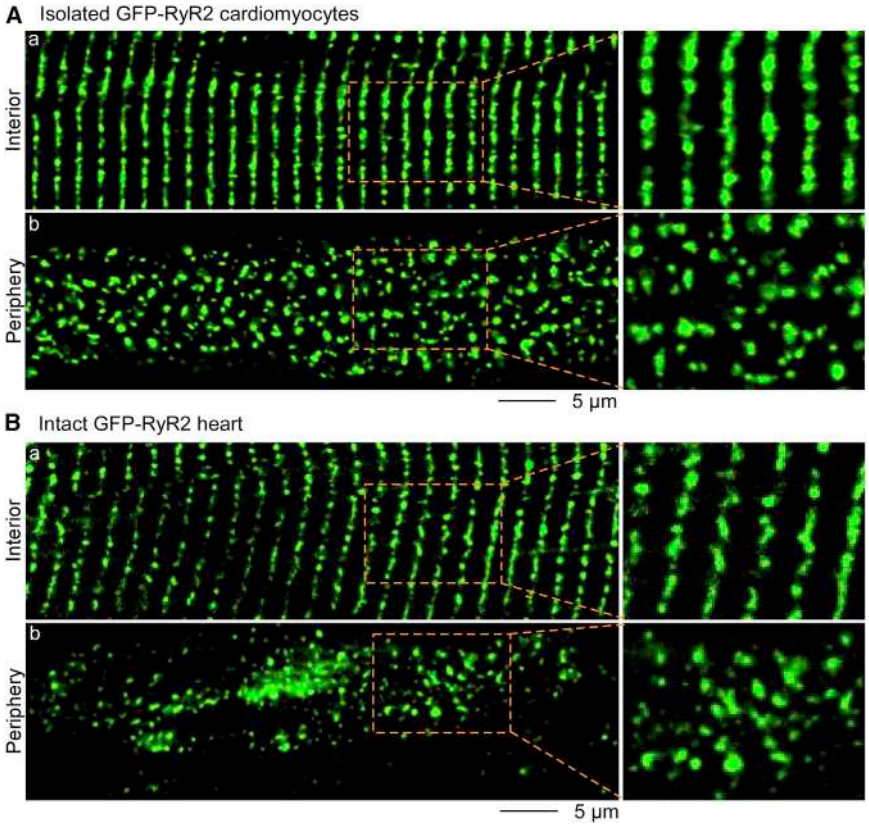

FIGURE 1 Different distributions of GFP-RyR2 clusters in the periphery and interior of live isolated ventricular myocytes and intact hearts. Representative confocal images are from the *z*-stack of (*A*) live ventricular myocytes ($n = 10$) and (*B*) intact hearts ($n = 14$ scans from three hearts) isolated from mice expressing a GFP-tagged RyR2. Imaging focusing on the interior showed highly ordered arrays of GFP-RyR2 clusters (*green puncta*) with clear single transverse rows in both live isolated cells and tissue (*Aa* and *Ba*). In contrast, optical confocal *z*-planes near the periphery showed irregular distribution of RyR2 clusters within the same cell/tissue (*Ab* and *Bb*). Enlarged images of selected areas are shown on the right. To see this figure in color, go online.

manner in the interior, but in an irregular pattern in the periphery of live ventricular myocytes.

Distribution of RyR2 clusters in the interior and periphery assessed using a TIRF microscope

Previous TIRF studies reported organized arrangements of RyR2 clusters as double rows in the cell periphery of fixed and permeabilized ventricular myocytes (29,30), which is different from the arrangement observed in GFP-RyR2 expressing cells (Fig. 1). To compare the imaging data, we also employed a TIRF microscope to determine the distribution of GFP-RyR2s in different subcellular layers within the same live ventricular myocyte. As shown in Fig. 2 *Aa*, S1 *A*, and S2 *A*, imaging with epi-fluorescent illumination that was focused on the interior showed highly ordered, single-row arrays of GFP-RyR2 clusters. HILO illumination (angle $<$ critical angle) showed arrays of GFP-RyR2 clusters in intermediate layers (Figs. 2 *Ab* and S2 *B*). TIRF imaging of the same cell showed irregular distribution of GFP-RyR2 clusters in the periphery (Figs. 2 *Ac*, S1 *A*, and S2 *A*). As a control, ventricular myocytes isolated from wild-type littermate mouse hearts yielded no detectable fluorescence signal under the identical imaging conditions (Fig. S1 *B*). As shown in Fig. 2 *B*, 2D Fourier transformations were derived from the respective fluorescence images. Distinct maxima were observed in the transforms in the interior (Figs. 2 *Ba* and S3) and intermediate layers (Fig. 2 *Bb*). In contrast, peripheral GFP-RyR2 clusters did not show intensity peaks in Fourier space (Figs. 2 *Bc* and S3). Quantitative comparison of image sets from 13 cells is shown in Fig. 2 *C*. These data indicate the absence of patterns/regularity of GFP-RyR2 clusters in the periphery and the presence of ordered GFP-RyR2 distribution in the intermediate layers and interior of the same ventricular myocyte. Note that irregularly distributed peripheral RyR2 clusters were observed in the presence or absence of laminin used for coating the glass coverslips to facilitate cell attachment (Fig. S3, *G* and *H*). Also note that although our TIRF imaging did not detect the double-row pattern of distribution of RyR2 clusters, HILO illumination did reveal the presence of RyR2 clusters with the double-row pattern of distribution (Fig. S2 *B*). These observations suggest that RyR2 clusters with the double-row pattern of distribution are located more interiorly than the irregularly distributed RyR2 clusters.

Dynamics of RyR2 clusters in the periphery and interior of live ventricular myocytes

To determine whether there are dynamic changes in RyR2 cluster distribution, we recorded time-lapse image series of interior and peripheral GFP-RyR2 clusters using a TIRF microscope. As shown in Fig. 3 *A*, nearly all

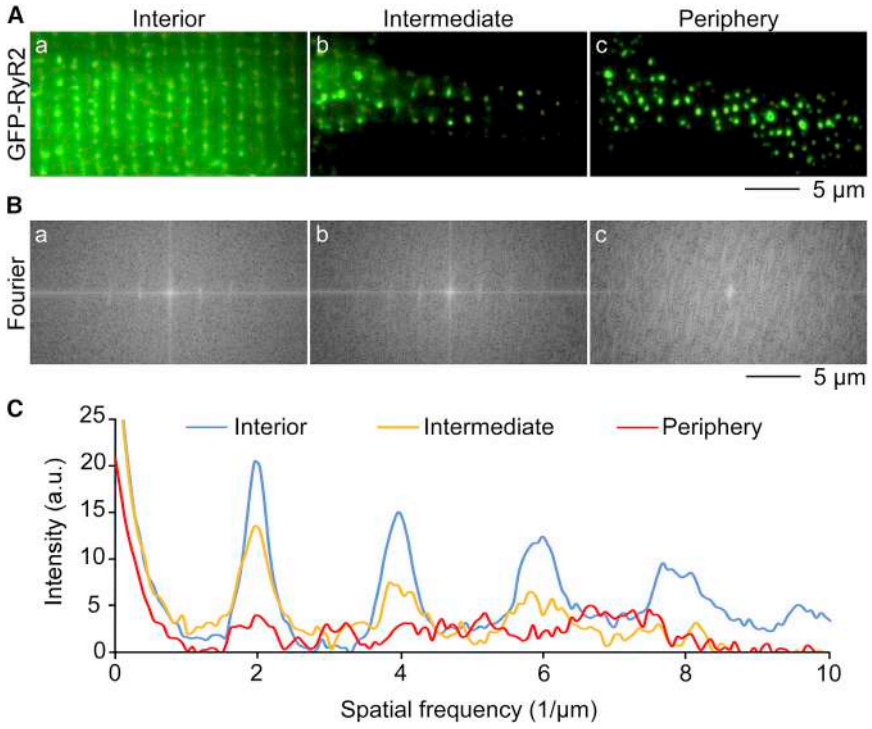

FIGURE 2 TIRF imaging of the distribution of GFP-RyR2 clusters. Fluorescence images (*A*) and corresponding 2D Fourier transforms (*B*) of different layers within the same ventricular myocytes isolated from GFP-RyR2 mice are represented. Imaging of epi-fluorescent illuminated (angle = 0) interior showed highly ordered, single-row arrays of GFP-RyR2 clusters (*Aa*). Highly inclined and laminated optical sheet illumination (angle < critical angle) of the same cell displayed arrays of GFP-RyR2 clusters with intercalated units in intermediate layers (*Ab*). Irregular distribution of GFP-RyR2 clusters was found in the periphery through TIRF imaging (*Ac*). Distinct maxima were observed in representative Fourier space of the interior (*Ba*) and intermediate layers (*Bb*). In contrast, Fourier transform of the TIRF image of peripheral GFP-RyR2 clusters did not reveal intensity peaks (*Bc*). Quantitative pattern comparison of different layers within the same cell (n = 13 cells) is shown in (*C*). To see this figure in color, go online.

GFP-RyR2 clusters in the interior appeared to be stationary under our imaging conditions. Similarly, the majority of peripheral GFP-RyR2 clusters appeared to remain at stable positions (Fig. 3 *B a–g*, *blue tracks*). However, movements were observed with some RyR2 clusters in the periphery. As indicated in Fig. 3 *B*, translocation of GFP-RyR2 clusters along the z axis was observed as dis/reappearance of GFP-RyR2 signals (Fig. 3 *B a–c*, zoom: z-Translocation, *pink dashed circle*). GFP-RyR2 cluster fusion (Fig. 3 *B d* and *e*, zoom: Fusion, *turquois dashed circle*) and unit separation (Fig. 3 *B b–e*, zoom: *purple dashed circle*) were also detected as GFP fluorescence signal merging/splitting. Additionally, considerable *xy* movements were observed (Fig. 3 *B f*, *red track*). These observations indicate that, unlike interior RyR2 clusters, peripheral RyR2 clusters display dynamic movements that are readily detectable under our imaging conditions.

To determine whether the movements of these peripheral RyR2 clusters are regulatable, we assessed the impact of reduced extracellular Ca^{2+}, caffeine (a RyR2 agonist), and tetracaine (a RyR2 inhibitor) on the movements of peripheral RyR2 clusters using time-lapse TIRF imaging (Fig. 4). We found that tetracaine (2 mM) dramatically diminished the fraction of cells that displayed cluster movements (Fig. 4, *A* and *B*). Furthermore, reducing the extracellular Ca^{2+} concentration from 2 to 0.5 mM markedly decreased the fraction of cells that showed cluster movements (Fig. 4 *C*). Interestingly, the effect of reduced extracellular Ca^{2+} on cluster movements could be reversed by the addition of caffeine (1 mM) (Fig. 4 *D*). These data indicate that the movements of these irregularly distributed peripheral RyR2 clusters are affected by Ca^{2+} and other RyR2 modulators, suggesting that the movement of these peripheral RyR2 clusters may be regulated by their own activities.

Confocal imaging of Ca^{2+} release at the interior and peripheral RyR2 clusters

Our recent studies showed the distribution and function of RyR2 clusters in the interior of ventricular myocytes (39). However, whether peripheral RyR2 clusters with an irregular pattern of distribution function with Ca^{2+} release properties are similar to those of interior RyR2 clusters is unclear. To address this question, we determined and compared local nonpropagating spontaneous Ca^{2+} release events at the peripheral and interior GFP-RyR2 clusters within the same cells. We employed high-speed confocal imaging to simultaneously record GFP-RyR2 locations and Rhod 2-AM signals in the interior and peripheral focal planes of the same myocytes. As shown in Fig. 5 *A*, highly ordered arrays of GFP-RyR2 clusters were found in the interior. In contrast, peripheral focus showed irregular distribution of GFP-RyR2 clusters. Spontaneous elementary release events, Ca^{2+} sparks, were clearly detected at the GFP-RyR2 cluster locations as small spatiotemporally restricted small increases in Rhod 2 fluorescence intensity (Fig. 5 *A*, *dashed orange circles*). Fig. 5 *B* shows quantitative comparison of elementary Ca^{2+} release characteristics, including 1) amplitude, 2) rate-of-rise, 3) duration at half-maximum, and

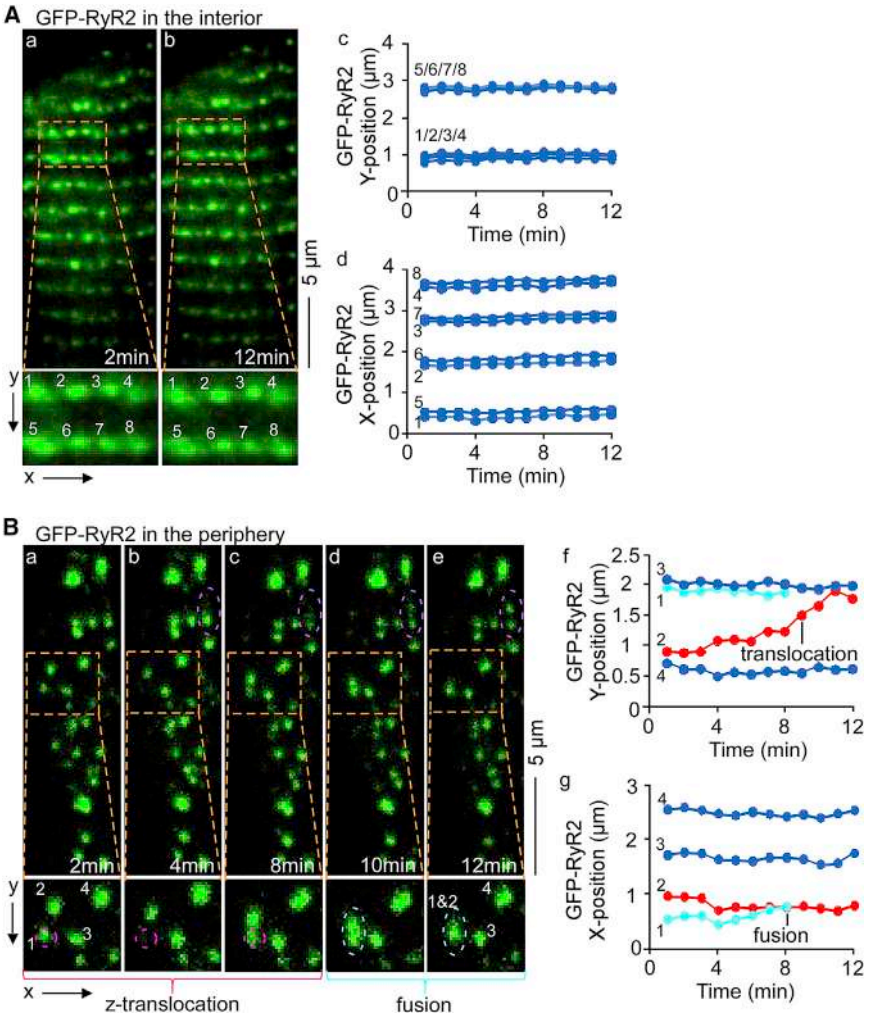

FIGURE 3 Time-lapse TIRF imaging of dynamics of GFP-RyR2 clusters in the periphery and interior of live ventricular myocytes. Representative images are given from time-lapse series of interior and peripheral GFP-RyR2 clusters, recorded using a TIRF microscope. Arrays of ordered GFP-RyR2 clusters were found in the interior. All GFP-RyR2 fluorescence signals (clusters *1–8*) in the interior remained stationary (*A*, *a* and *b*). TrackMate advanced cluster dynamic analysis showed only minimal *x*-, *y*-signal movements (*A*, *c* and *d*, *blue tracks*). In contrast, distribution of signals appeared disordered in the periphery (*B*, *a–e*). The majority of peripheral GFP-RyR2 signals remained at same positions (*B*, *a–e*; *f* and *g*, *blue tracks*). However, multiple clusters displayed dynamic movements: 1) Translocation along the *z* axis (*B*, *a–c*, zoom: *pink dashed circle*); 2) GFP-RyR2 cluster fusion (*B*, *d* and *e*, zoom: *turquoise dashed circle*); and 3) unit separation (*B*, *b–e*, zoom: *purple dashed circle*). Additionally, TrackMate analysis showed major *xy* movement (*B*, *f*, *red track*) ($n = 5$ cells). To see this figure in color, go online.

4) decay time, observed in the periphery and interior of the same cells. These data demonstrate that peripheral RyR2 clusters with an irregular pattern of distribution are functional with a Ca^{2+} release profile similar to that of interior RyR2 clusters.

Ca^{2+} release at the interior and peripheral RyR2 clusters assessed by a TIRF microscope

Confocal imaging allows only diffraction-limited optical sectioning (31,32). To overcome this limitation, we employed a TIRF microscope in the TIRF mode. We recorded spontaneous Ca^{2+} release events at GFP-RyR2 clusters in the interior and periphery of the same ventricular myocytes. As shown in Fig. 6 *A*, image series of the interior and periphery showed GFP-RyR2 clusters as stationary fluorescence peaks throughout the recording. In contrast, Ca^{2+} release events were detected as temporally and spatially restricted intensity fluctuations of the cytosolic Ca^{2+} indicator (Fluo4-AM) fluorescence. Ca^{2+} sparks appeared clearly at GFP-RyR2 clusters (Fig. 6 *A*, *dashed red circles*). Analysis of Ca^{2+} release characteristics, including 1) amplitude, 2) rate-of-rise, 3) duration at half-maximum, and 4) decay time, observed in the periphery and interior of the same cells are summarized in Fig. 6 *B*. These data further support the notion that the irregularly distributed RyR2 clusters in the periphery function with a Ca^{2+} release profile similar to that of RyR2 clusters in the interior of live ventricular myocytes. Thus, both the confocal and TIRF imaging studies demonstrate that the characteristics of Ca^{2+} sparks detected in the interior and periphery are similar. This similarity suggests that a major portion of the Ca^{2+} signals detected in the periphery are unlikely to be due to the diffusion of Ca^{2+} from Ca^{2+} sparks originated from the interior.

DISCUSSION

The distribution of RyR2 clusters (the Ca^{2+} release units) is believed to be a critical determinant of controlled Ca^{2+} release and thus, the stability of EC coupling in the heart. Although the distributions and functions of RyR2 clusters

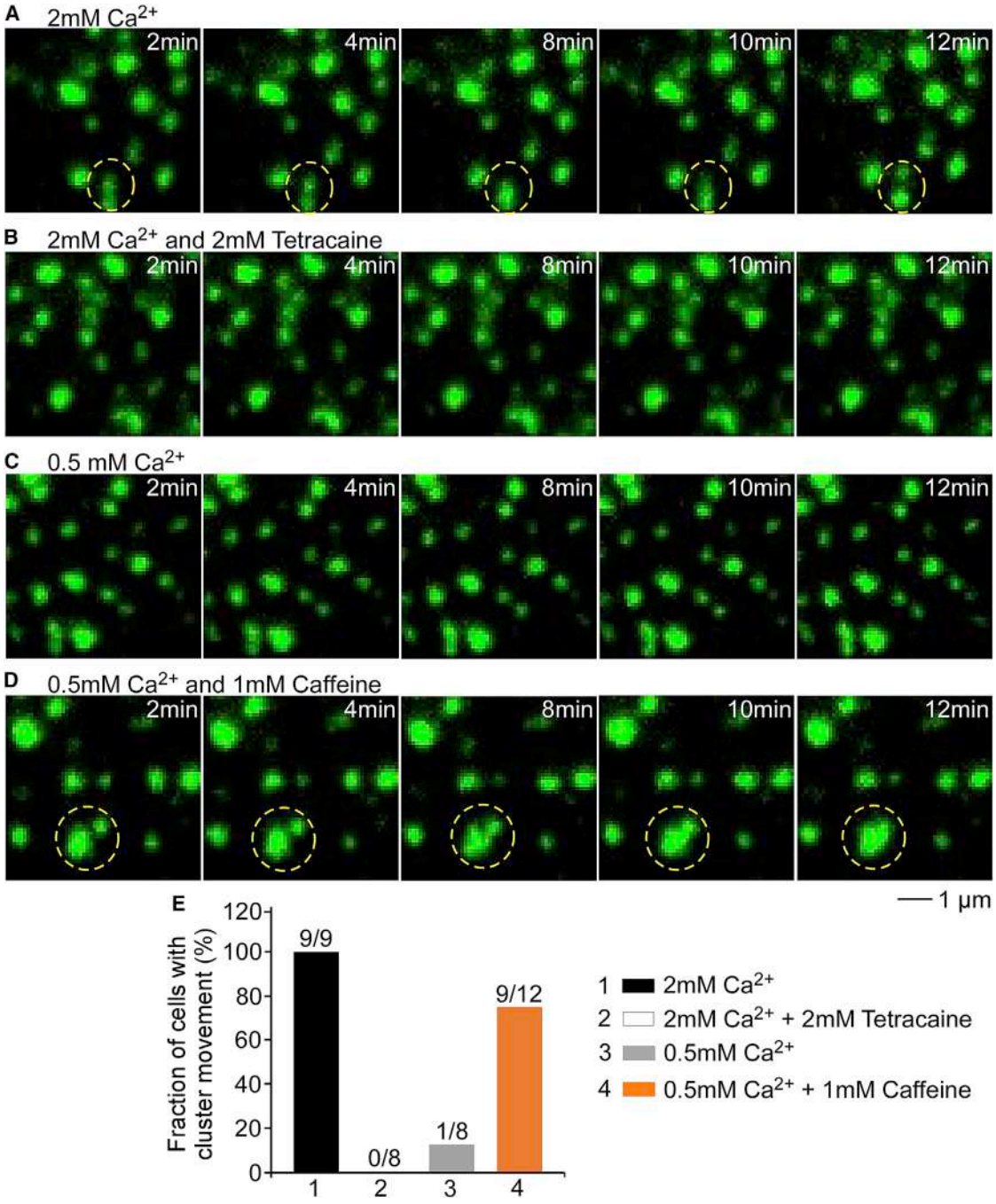

FIGURE 4 Movements of GFP-RyR2 clusters in the periphery of live ventricular myocytes are affected by RyR2 modulators. Representative images from time-lapse TIRF series of peripheral GFP-RyR2 clusters were recorded in the presence of (*A*) 2 mM extracellular Ca^{2+}, (*B*) 2 mM extracellular Ca^{2+} plus 2 mM tetracaine, (*C*) 0.5 mM extracellular Ca^{2+}, and (*D*) 2 mM extracellular Ca^{2+} plus 1 mM caffeine. Representative GFP-RyR2 cluster separation/fusion is highlighted (*yellow dashed circles*). (*E*) Given here is the fraction of cells that showed GFP-RyR2 cluster movement ($n = 8$–9 cells). To see this figure in color, go online.

in the interior of cardiomyocytes have been extensively studied, the distribution and function of RyR2 clusters in the periphery is poorly understood. This is in part due to the difficulty in imaging the distribution and function of peripheral RyR2 clusters. In this study, we employed a unique knock-in mouse model expressing a GFP-tagged RyR2 to determine the distribution and function of GFP-RyR2 clusters in the periphery of live ventricular myocytes using confocal and TIRF microscopy. We found that unlike the interior RyR2 clusters that are organized in a highly ordered striated pattern with little detectable movement, the peripheral RyR2 clusters are organized in

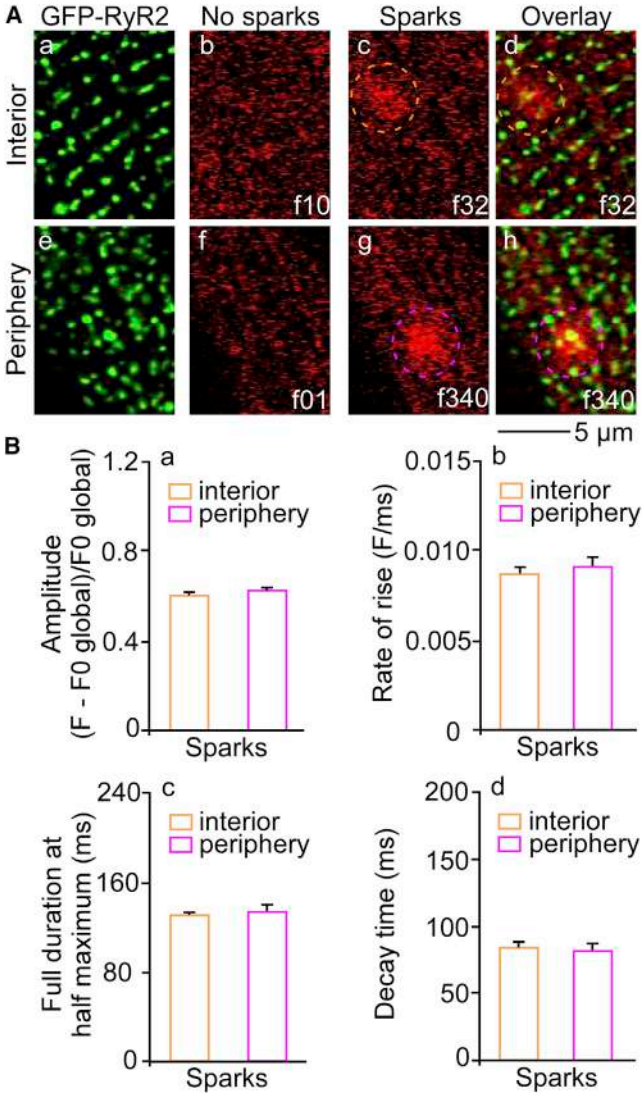

FIGURE 5 Confocal imaging of spontaneous Ca^{2+} release events at GFP-RyR2 clusters in the interior and periphery within the same ventricular myocytes. High-speed confocal imaging of spontaneous Ca^{2+} release (*red fluorescence*) at GFP-RyR2 clusters (*green puncta*) at the interior and peripheral confocal focus planes of the same ventricular myocyte is presented in (*A*). Distribution of GFP-RyR2 clusters in the interior was found to be highly ordered, contrasting irregular patterns at the periphery (*GFP-RyR2*). Ca^{2+} sparks were detected at GFP-RyR2 locations as spatiotemporally restricted small increases in Rhod-2 fluorescence intensity. Quantitative comparison of characteristics of elementary Ca^{2+} release at RyR2 clusters (*a*) amplitude; (*b*) rate-of-rise; (*c*) duration at half maximum; and (*d*) decay time; ($n = 16$ cells; 927 Ca^{2+} spark events in interior and 774 Ca^{2+} spark events in the periphery; *f*, frame) is shown in (*B*). To see this figure in color, go online.

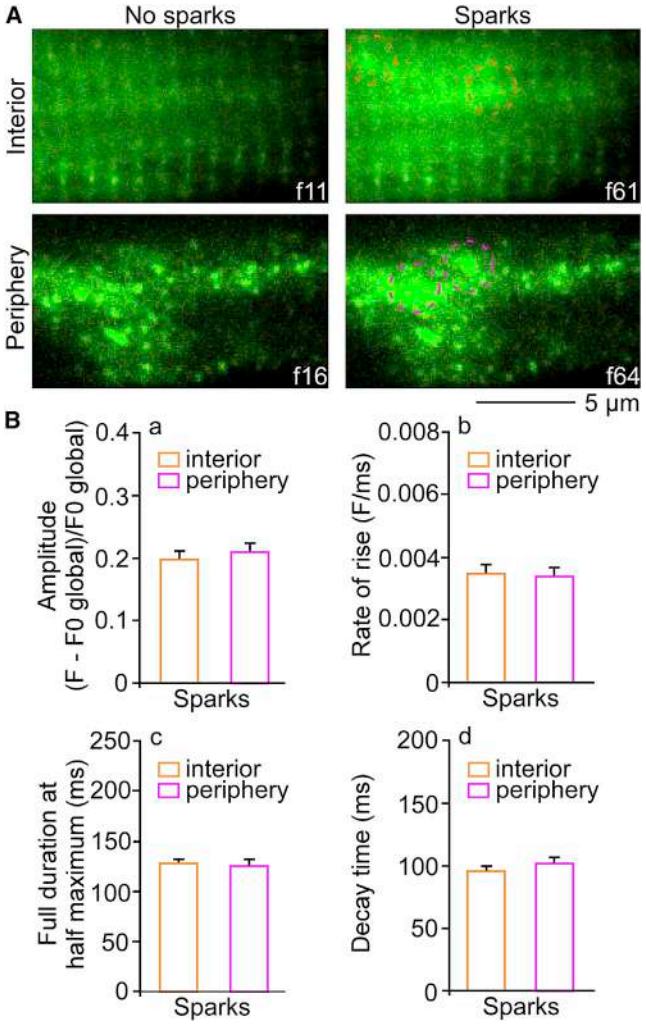

FIGURE 6 TIRF and HILO imaging of spontaneous Ca^{2+} release events at GFP-RyR2 clusters in the interior and periphery within the same ventricular myocytes. Spontaneous Ca^{2+} release at GFP-RyR2 clusters was recorded in the interior and periphery of the same ventricular myocyte with a TIRF microscope. Images from the time series (50–60 FPS) of GFP-RyR2 clusters were observed as stationary fluorescence peaks throughout the recording, as displayed. Their distribution appeared highly ordered in the interior and disordered in the periphery of the same cell (*A*). Ca^{2+} sparks appeared clearly at GFP-RyR2 clusters as transient and spatially restricted elevations in fluorescence signals (*A*). Quantitative comparison of characteristics of elementary Ca^{2+} release at RyR2 clusters (*a*) amplitude; (*b*) rate-of-rise; (*c*) duration at half maximum; and (*d*) decay time are shown ($n = 10$ cells; 1872 Ca^{2+} sparks in interior and 4153 Ca^{2+} sparks in periphery; *f*, frame) is shown in (*B*). To see this figure in color, go online.

an irregular pattern with dynamic movements that are affected by RyR2 modulators. Importantly, the irregularly distributed peripheral RyR2 clusters are functional with a Ca^{2+} release profile similar to that in the interior. However, the physiological significance of these irregularly distributed peripheral RyR2 clusters has yet to be defined.

Discrepancies regarding the distribution of peripheral RyR2 clusters

Previous studies have shown two different patterns of distribution of RyR2 clusters in the peripheral region of ventricular myocytes. 3D confocal microscopy showed disordered distribution of RyR2 clusters in the outermost optical confocal *z*-planes (26–28). In contrast, RyR2 clusters displayed a double-row feature in images obtained by

TIRF microscopy (29,30). The exact reasons for this discrepancy are unclear. Differences in sample preparation and/or antibody binding conditions may account for these different observations. Furthermore, the optical sectioning capability of the imaging techniques used differs. On the one hand, employment of pinholes in confocal microscopy can only restrict light collection to optical segments >500 nm in thickness (31,32). Thus, the observed irregular pattern of RyR2 clusters may reflect combined signals from multiple layers near, but not exclusively from, the periphery. On the other hand, evanescent fields generated during TIRF imaging illuminate only the near-field (~100 nm) (31,32). Thus, only fluorophores in close proximity to the cell surface at the cell-glass coverslip interface are excited and imaged. Therefore, one would expect that the periphery just beneath the plasma membrane is occupied by double-rows of RyR2 clusters. However, we found an irregular pattern of distribution of GFP-RyR2 clusters using both the confocal and TIRF imaging in the periphery of live ventricular myocytes. And we also observed double rows of RyR2 clusters using HILO illumination. Together, these observations suggest that double rows of RyR2 clusters are located more interiorly than the irregularly distributed RyR2 clusters.

A possible reason for the differences between our study and former TIRF studies (29,30) may be due to the use of fixed and permeabilized cardiomyocytes versus live ventricular myocytes in this study. In our experience, we found that live ventricular myocytes adhere readily to the glass coverslips, forming multiple contacts with the surface of the coverslips, whereas, fixed and permeabilized cells did not adhere to the glass coverslips. The lack of contact of fixed and permeabilized cells to the surface of coverslips would make TIRF imaging of the cell periphery difficult. To circumvent this problem, Jayasinghe et al. (29) embedded fixed myocytes in agarose blocks. These blocks were permeabilized, stained with anti-RyR2 antibody, and mounted for TIRF imaging. Another TIRF study (30) used antibody-labeled, fixed and permeabilized cells in suspension. It is important to note that in both studies, the fixed, permeabilized cells were stacked between two coverslips. However, whether agarose embedding and/or application of mechanical forces affects the distribution of peripheral RyR2 clusters is unclear. The peripheral layers could have been altered and/or shifted out of the TIRF detection range by these mechanical stresses. In this regard, our live cell imaging approach revealed in situ distribution of RyR2 clusters in the periphery of living and excitable cardiomyocytes.

It should be noted that the areas detected by TIRF imaging are much smaller than the areas of the cells, and the shapes of the illuminated areas are always irregular. This is expected if the areas detected by TIRF reflect the areas of the live cells contacting the glass coverslip. The small size and irregularity of the contact areas would make the detection of long-range orderliness/patterns difficult, if not impossible. This also raises an important question of whether the contact areas detected by TIRF are large enough to determine the relative orderliness of the distribution of RyR2 clusters located in different regions of the cell. To address this question, we performed Fourier transformation of fluorescence images obtained from the interior and peripheral areas with different sizes. We found that an epi-fluorescent image from the interior with an area as small as 5.5×3.5 μm is sufficient to reveal intensity peaks (orderliness). On the other hand, a TIRF image from the periphery with the same area showed no intensity peaks (Fig. S3, *A–F*). Note that the TIRF images yield brighter signals and more detailed Fourier transforms than epi-fluorescent images. Thus, the absence of peaks in the Fourier space of TIRF images is unlikely due to optical differences in the detection techniques. Therefore, although it may not be large enough to detect long-range orderliness/patterns, the peripheral contact area detected by TIRF ($>5.5 \times 3.5$ μm) is large enough to assess the orderliness of peripheral RyR2 clusters relative to that in the interior.

There are also other factors that may potentially affect the distribution of RyR2 clusters in the periphery. For instance, the use of laminin may affect the adhesion of live cardiomyocytes to the glass coverslip and hence the pattern of distribution of RyR2 clusters in the periphery. To test this possibility, we compared the patterns of distribution of peripheral GFP-RyR2 clusters in the presence and absence of laminin. We found an irregular pattern of distribution of GFP-RyR2 clusters in the periphery in the presence or absence of laminin (Fig. S3, *G* and *H*), different from that in the interior. Therefore, it is unlikely that the irregular pattern of distribution of RyR2 clusters observed in the periphery is due to the use of laminin. In addition, it is possible that the pattern of distribution of RyR2 clusters in the periphery may vary from species to species. In this study, we employed cardiomyocytes isolated from the GFP-RyR2 knock-in mice, whereas rat or rabbit cardiomyocytes were used in other studies (26–30). However, it is important to note that the irregularly distributed RyR2 clusters were also observed in the peripheral region of rat and rabbit cardiomyocytes in other studies (26,27). Hence, mouse, rat, and rabbit cardiomyocytes express these irregularly distributed RyR2 clusters in the peripheral region of the cell. It is also possible that the insertion of GFP into the RyR2 sequence may affect the distribution of peripheral RyR2 clusters. However, the insertion of GFP does not seem to significantly alter the distribution of RyR2 clusters in the interior. Furthermore, as mentioned above, irregularly distributed non-GFP-labeled, native RyR2 clusters have also been detected in the periphery of rat and rabbit cardiomyocytes (26,27). Hence, the irregular pattern of distribution of GFP-tagged RyR2 clusters observed in our GFP-RyR2 mouse cardiomyocytes is unlikely to be a

region-specific artifact that resulted from the insertion of GFP.

Movements of RyR2 clusters

Chen-Izu et al. (27) and Jayasinghe et al. (29) suggested that RyR2 trafficking and protein turnover potentially have led to the different peripheral patterns of distribution of RyR2 clusters in antibody-stained ventricular myocytes. Cell fixation might have captured a snapshot of the migration of RyR2 clusters from the interior toward the surface along the SR membrane system (and vice versa). However, our time-lapse TIRF imaging revealed that the majority of irregularly distributed GFP-RyR2 clusters were stationary in the periphery of live ventricular myocytes. Also, all GFP-RyR2 clusters in the interior of these cells showed few detectable movements during the entire recording period (>20 min). Thus, the irregular distribution of peripheral RyR2 clusters is unlikely to be the consequence of trafficking of all superficial clusters. Furthermore, the peripheral RyR2 clusters that underwent dynamic movements were closely localized with those stationary RyR2 clusters. Thus, it is unlikely that the movement of these RyR2 clusters resulted from movement induced by a patch of cell membrane. Such membrane movements would be expected to affect a large membrane area, which would simultaneously affect the movement of many closely juxtaposed RyR2 clusters. However, this is clearly not the case. We observed *x*-, *y*-, and *z*-directed translocation of GFP-RyR2 clusters. We also observed fusion, or separation, of GFP-RyR2 clusters in the periphery. Importantly, we found that these movements are affected by extracellular Ca^{2+} concentrations and the RyR2 activator (caffeine) and inhibitor (tetracaine). These observations suggest that the movement of irregularly distributed RyR2 clusters in the periphery is a regulated process. The detailed mechanism underlying these complex dynamic movements of peripheral RyR2 clusters has yet to be defined.

It is important to point out that it is much more difficult to detect movements of RyR2 clusters located in the cell interior. The interior RyR2 clusters are likely to be confined to the small area of the narrow t-tubules. It is also hard to resolve RyR2 clusters located deeper into the myocytes due to lower *z*-resolution and optical aberrations. Therefore, under our imaging conditions, we cannot rule out that interior RyR2 clusters may also undergo dynamic movements. In this regard, it is of interest to note that RyR2 tetramers within a cluster are mobile (42). It is also important to know that each RyR2 cluster may contain multiple smaller clusters (30). Thus, each of the GFP fluorescent spots observed in our study could be composed of multiple clusters of RyR2, which is consistent with our observations that GFP-RyR2 clusters detected in the periphery can undergo fusion into a larger cluster or separation into smaller clusters.

Function and relevance of peripheral RyR2 clusters

The distribution of RyR2 clusters is believed to be an important determinant of normal Ca^{2+} release in the heart. Highly ordered arrays of RyR2s in the interior are proposed to underlie stable, graded CICR during ECC. However, little is known about the functional relevance of peripheral RyR2 clusters. On the one hand, Dan et al. (26) showed that during cardiomyocyte maturation the distribution of RyR2 clusters in the periphery changed dramatically. Local nonuniformities in the growth of sarcomeres has been proposed to underlie the appearance of dislocated RyR2s (27,43). Thus, one might speculate that these irregularly distributed RyR2 clusters in the periphery reflect those observed in early development. On the other hand, peripheral RyR2 clusters have been suggested to be involved in centripetally propagating Ca^{2+} release (26). Spacing between functional RyR2 units in the periphery of cardiomyocytes has also been suggested to be a determinant of the probability of initiation of global Ca^{2+} waves (20). However, despite these functional implications, it has remained unclear whether peripheral RyR2 clusters with an irregular pattern of distribution are functional and have Ca^{2+} release properties similar to those of interior RyR2 clusters. Our confocal and TIRF recordings of Ca^{2+} release at RyR2 clusters in the periphery demonstrated that irregularly distributed peripheral RyR2 clusters are indeed functional. Furthermore, we showed that peripheral RyR2 clusters possess the same Ca^{2+} release profile as clusters in the interior. Therefore, peripheral RyR2 clusters may play a role in determining the Ca^{2+} release profiles in the region just beneath the cell surface of ventricular myocytes.

Irregular distribution of RyR2 clusters has been observed in the setting of cardiac hypertrophy and heart failure (44). This irregular distribution of RyR2 clusters has been implicated in the generation of Ca^{2+} waves and triggered arrhythmias. However, we found irregular distribution of functional RyR2 Ca^{2+} release units in the periphery of live, presumably healthy, cardiomyocytes. Thus, by itself, irregular submembrane distribution of RyR2 clusters does not necessarily associate with cardiac pathology. It may have a potentially unique physiological role in Ca^{2+} signaling in cardiac cells, which remains to be investigated.

CONCLUSIONS

In this study, we employed a GFP-tagged RyR2 mouse model to compare the distribution and function of RyR2 clusters in the periphery and interior of live ventricular myocytes. We found that the distribution of RyR2 clusters in the periphery is irregular and dynamic, different from those in the interior. We also demonstrated that peripheral RyR2 clusters form functional Ca^{2+} release units with a

similar Ca^{2+} release profile to those found in the interior. Our results provide, to our knowledge, novel insights into the distribution and function of RyR2 clusters in the periphery of intact cardiomyocytes.

SUPPORTING MATERIAL

Three figures are available at http://www.biophysj.org/biophysj/supplemental/S0006-3495(17)31258-4.

AUTHOR CONTRIBUTIONS

F.H., P.D., M.A., R.B., L.H.-M., and S.R.W.C. designed research. F.H., P.D., and A.G., performed research. F.H., C.N., A.V., H.E.D.J.K., R.B., L.H.-M., and S.R.W.C. analyzed data. F.H., P.D., C.N., A.V., H.E.D.J.K., R.B., L.H.-M., and S.R.W.C. wrote the article.

ACKNOWLEDGMENTS

We thank Dr. James D. McGee, Departments of Biochemistry & Molecular Biology, Medical Genetic, and the Microscopy and Imaging Facility (MIF) at the University of Calgary, for the use of their imaging systems.

This work was supported by research grants from the Canadian Institutes of Health Research, the Heart and Stroke Foundation of Canada, the Canada Foundation for Innovation, the Natural Sciences and Engineering Research Council of Canada, and the Heart and Stroke Foundation Chair in Cardiovascular Research (to S.R.W.C.). This study was also supported by the Spanish Ministry of Economy and Competitiveness SAF2014-58286-C2-1-R (to L.H.-M.) and DPI2013-44584-R (to R.B.).

REFERENCES

1. Bers, D. M. 2001. Excitation-Contraction Coupling and Cardiac Contractile Force, 2nd Ed. Kluwer/Springer, Dordrecht, The Netherlands.
2. Bers, D. M. 2002. Cardiac excitation-contraction coupling. *Nature.* 415:198–205.
3. Cannell, M. B., H. Cheng, and W. J. Lederer. 1995. The control of calcium release in heart muscle. *Science.* 268:1045–1049.
4. Cannell, M. B., and C. Soeller. 1997. Numerical analysis of ryanodine receptor activation by L-type channel activity in the cardiac muscle diad. *Biophys. J.* 73:112–122.
5. Niggli, E., and W. J. Lederer. 1990. Voltage-independent calcium release in heart muscle. *Science.* 250:565–568.
6. Stern, M. D., and E. G. Lakatta. 1992. Excitation-contraction coupling in the heart: the state of the question. *FASEB J.* 6:3092–3100.
7. Stern, M. D. 1992. Theory of excitation-contraction coupling in cardiac muscle. *Biophys. J.* 63:497–517.
8. Sobie, E. A., K. W. Dilly, …, M. S. Jafri. 2002. Termination of cardiac Ca^{2+} sparks: an investigative mathematical model of calcium-induced calcium release. *Biophys. J.* 83:59–78.
9. Bassani, J. W., W. Yuan, and D. M. Bers. 1995. Fractional SR Ca release is regulated by trigger Ca and SR Ca content in cardiac myocytes. *Am. J. Physiol.* 268:C1313–C1319.
10. Stern, M. D., G. Pizarro, and E. Ríos. 1997. Local control model of excitation-contraction coupling in skeletal muscle. *J. Gen. Physiol.* 110:415–440.
11. López-López, J. R., P. S. Shacklock, …, W. G. Wier. 1994. Local, stochastic release of Ca^{2+} in voltage-clamped rat heart cells: visualization with confocal microscopy. *J. Physiol.* 480:21–29.
12. López-López, J. R., P. S. Shacklock, …, W. G. Wier. 1995. Local calcium transients triggered by single L-type calcium channel currents in cardiac cells. *Science.* 268:1042–1045.
13. Wier, W. G., T. M. Egan, …, C. W. Balke. 1994. Local control of excitation-contraction coupling in rat heart cells. *J. Physiol.* 474:463–471.
14. Franzini-Armstrong, C., F. Protasi, and V. Ramesh. 1999. Shape, size, and distribution of Ca^{2+} release units and couplons in skeletal and cardiac muscles. *Biophys. J.* 77:1528–1539.
15. Cheng, H., and W. J. Lederer. 2008. Calcium sparks. *Physiol. Rev.* 88:1491–1545.
16. Cheng, H., M. R. Lederer, …, W. J. Lederer. 1996. Excitation-contraction coupling in heart: new insights from Ca^{2+} sparks. *Cell Calcium.* 20:129–140.
17. Cheng, H., W. J. Lederer, and M. B. Cannell. 1993. Calcium sparks: elementary events underlying excitation-contraction coupling in heart muscle. *Science.* 262:740–744.
18. Smith, G. D., J. E. Keizer, …, H. Cheng. 1998. A simple numerical model of calcium spark formation and detection in cardiac myocytes. *Biophys. J.* 75:15–32.
19. Izu, L. T., Y. Xie, …, Y. Chen-Izu. 2013. Ca^{2+} waves in the heart. *J. Mol. Cell. Cardiol.* 58:118–124.
20. Izu, L. T., S. A. Means, …, C. W. Balke. 2006. Interplay of ryanodine receptor distribution and calcium dynamics. *Biophys. J.* 91:95–112.
21. Carl, S. L., K. Felix, …, D. G. Ferguson. 1995. Immunolocalization of sarcolemmal dihydropyridine receptor and sarcoplasmic reticular triadin and ryanodine receptor in rabbit ventricle and atrium. *J. Cell Biol.* 129:673–682.
22. Parker, I., W. J. Zang, and W. G. Wier. 1996. Ca^{2+} sparks involving multiple Ca^{2+} release sites along Z-lines in rat heart cells. *J. Physiol.* 497:31–38.
23. Asghari, P., M. Schulson, …, E. D. W. Moore. 2009. Axial tubules of rat ventricular myocytes form multiple junctions with the sarcoplasmic reticulum. *Biophys. J.* 96:4651–4660.
24. Soeller, C., D. Crossman, …, M. B. Cannell. 2007. Analysis of ryanodine receptor clusters in rat and human cardiac myocytes. *Proc. Natl. Acad. Sci. USA.* 104:14958–14963.
25. Jayasinghe, I. D., D. J. Crossman, …, M. B. Cannell. 2010. A new twist in cardiac muscle: dislocated and helicoid arrangements of myofibrillar z-disks in mammalian ventricular myocytes. *J. Mol. Cell. Cardiol.* 48:964–971.
26. Dan, P., E. Lin, …, G. F. Tibbits. 2007. Three-dimensional distribution of cardiac Na^{+}-Ca^{2+} exchanger and ryanodine receptor during development. *Biophys. J.* 93:2504–2518.
27. Chen-Izu, Y., S. L. McCulle, …, L. T. Izu. 2006. Three-dimensional distribution of ryanodine receptor clusters in cardiac myocytes. *Biophys. J.* 91:1–13.
28. Jayasinghe, I. D., D. Baddeley, …, C. Soeller. 2012. Nanoscale organization of junctophilin-2 and ryanodine receptors within peripheral couplings of rat ventricular cardiomyocytes. *Biophys. J.* 102:L19–L21.
29. Jayasinghe, I. D., M. B. Cannell, and C. Soeller. 2009. Organization of ryanodine receptors, transverse tubules, and sodium-calcium exchanger in rat myocytes. *Biophys. J.* 97:2664–2673.
30. Baddeley, D., I. D. Jayasinghe, …, C. Soeller. 2009. Optical single-channel resolution imaging of the ryanodine receptor distribution in rat cardiac myocytes. *Proc. Natl. Acad. Sci. USA.* 106:22275–22280.
31. Sanderson, M. J., I. Smith, …, M. D. Bootman. 2014. Fluorescence microscopy. *Cold Spring Harb. Protoc.* https://doi.org/10.1101/pdb.top071795.
32. Fish, K. N. 2009. Total internal reflection fluorescence (TIRF) microscopy. *Curr. Protoc. Cytom.* Chapter 12:Unit12.18.
33. Scriven, D. R. L., P. Asghari, …, E. D. W. Moore. 2010. Analysis of Cav1.2 and ryanodine receptor clusters in rat ventricular myocytes. *Biophys. J.* 99:3923–3929.

34. Sedarat, F., L. Xu, …, G. F. Tibbits. 2000. Colocalization of dihydropyridine and ryanodine receptors in neonate rabbit heart using confocal microscopy. *Am. J. Physiol. Heart Circ. Physiol.* 279:H202–H209.

35. Tokunaga, M., N. Imamoto, and K. Sakata-Sogawa. 2008. Highly inclined thin illumination enables clear single-molecule imaging in cells. *Nat. Methods.* 5:159–161.

36. Wang, S. Q., M. D. Stern, …, H. Cheng. 2004. The quantal nature of Ca^{2+} sparks and in situ operation of the ryanodine receptor array in cardiac cells. *Proc. Natl. Acad. Sci. USA.* 101:3979–3984.

37. Brette, F., L. Sallé, and C. H. Orchard. 2004. Differential modulation of L-type Ca^{2+} current by SR Ca2+ release at the T-tubules and surface membrane of rat ventricular myocytes. *Circ. Res.* 95:e1–e7.

38. Scriven, D. R. L., P. Dan, and E. D. W. Moore. 2000. Distribution of proteins implicated in excitation-contraction coupling in rat ventricular myocytes. *Biophys. J.* 79:2682–2691.

39. Hiess, F., A. Vallmitjana, …, S. R. W. Chen. 2015. Distribution and function of cardiac ryanodine receptor clusters in live ventricular myocytes. *J. Biol. Chem.* 290:20477–20487.

40. Chen, W., R. Wang, …, S. R. W. Chen. 2014. The ryanodine receptor store-sensing gate controls Ca^{2+} waves and Ca^{2+}-triggered arrhythmias. *Nat. Med.* 20:184–192.

41. Tinevez, J.-Y., N. Perry, …, K. W. Eliceiri. 2017. TrackMate: an open and extensible platform for single-particle tracking. *Methods.* 115:80–90.

42. Asghari, P., D. R. L. Scriven, …, E. D. W. Moore. 2014. Nonuniform and variable arrangements of ryanodine receptors within mammalian ventricular couplons. *Circ. Res.* 115:252–262.

43. Yu, J.-G., and B. Russell. 2005. Cardiomyocyte remodeling and sarcomere addition after uniaxial static strain in vitro. *J. Histochem. Cytochem.* 53:839–844.

44. Song, L.-S., E. A. Sobie, …, H. Cheng. 2006. Orphaned ryanodine receptors in the failing heart. *Proc. Natl. Acad. Sci. USA.* 103:4305–4310.

Biophysical Journal, Volume *114*

Supplemental Information

Dynamic and Irregular Distribution of RyR2 Clusters in the Periphery of Live Ventricular Myocytes

Florian Hiess, Pascal Detampel, Carme Nolla-Colomer, Alex Vallmitjana, Anutosh Ganguly, Matthias Amrein, Henk E.D.J. ter Keurs, Raul Benítez, Leif Hove-Madsen, and S. R. Wayne Chen

Supplemental Fig. 1

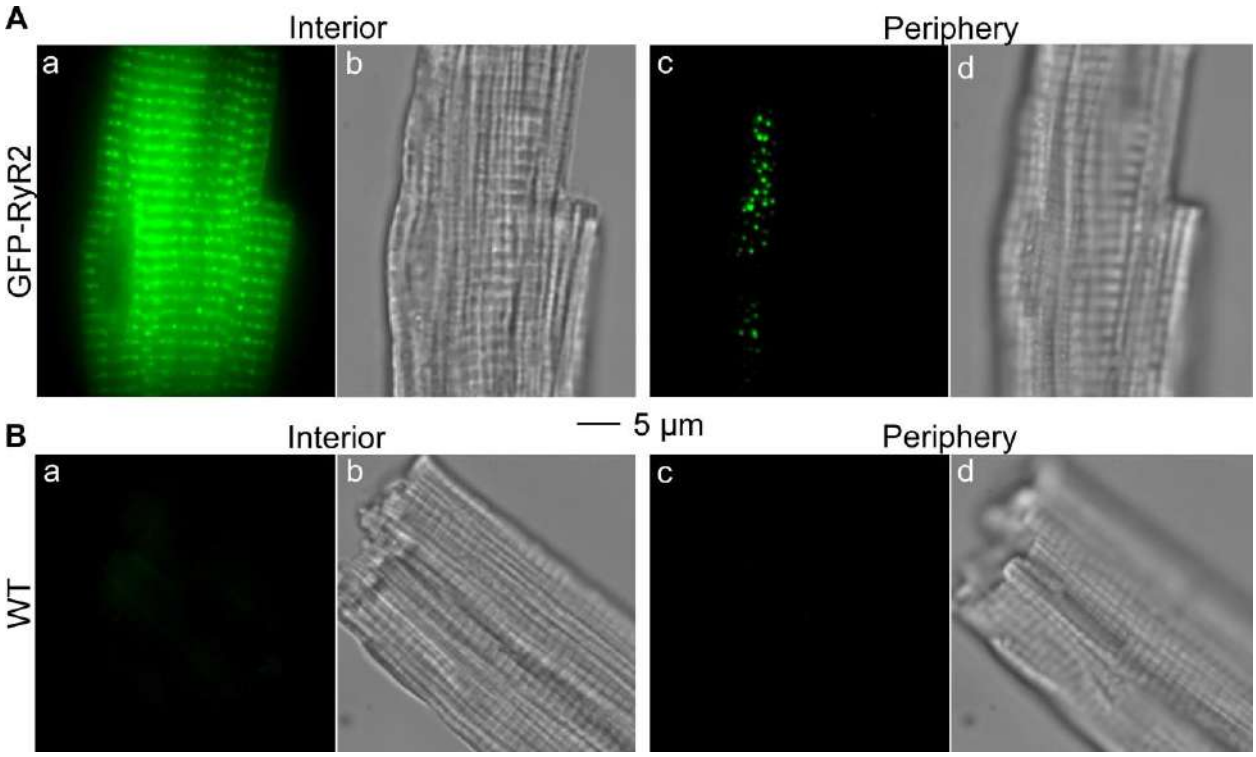

Supplemental Fig. 1. Fluorescence Signal Detection with a TIRF Microscope in the Interior and Periphery of Ventricular Myocytes Isolated from GFP-RyR2 Mice and WT Littermates

Representative fluorescence and transmission light images were taken under the same conditions in the same live ventricular myocytes isolated from GFP-RyR2 knock-in mice (A), or WT control littermate (B). GFP-fluorescence was only detected in myocytes isolated from the GFP-RyR2 knock-in mice, but not in WT mice (a & c). Membrane integrity and typical rod-shaped appearance in transmission light images indicate cell viability and allowed comparison of optical focus planes (b & d). (n = 6 GFP-RyR2 expressing cells and 15 WT cells) Scale bar applies to all images.

Supplemental Fig. 2

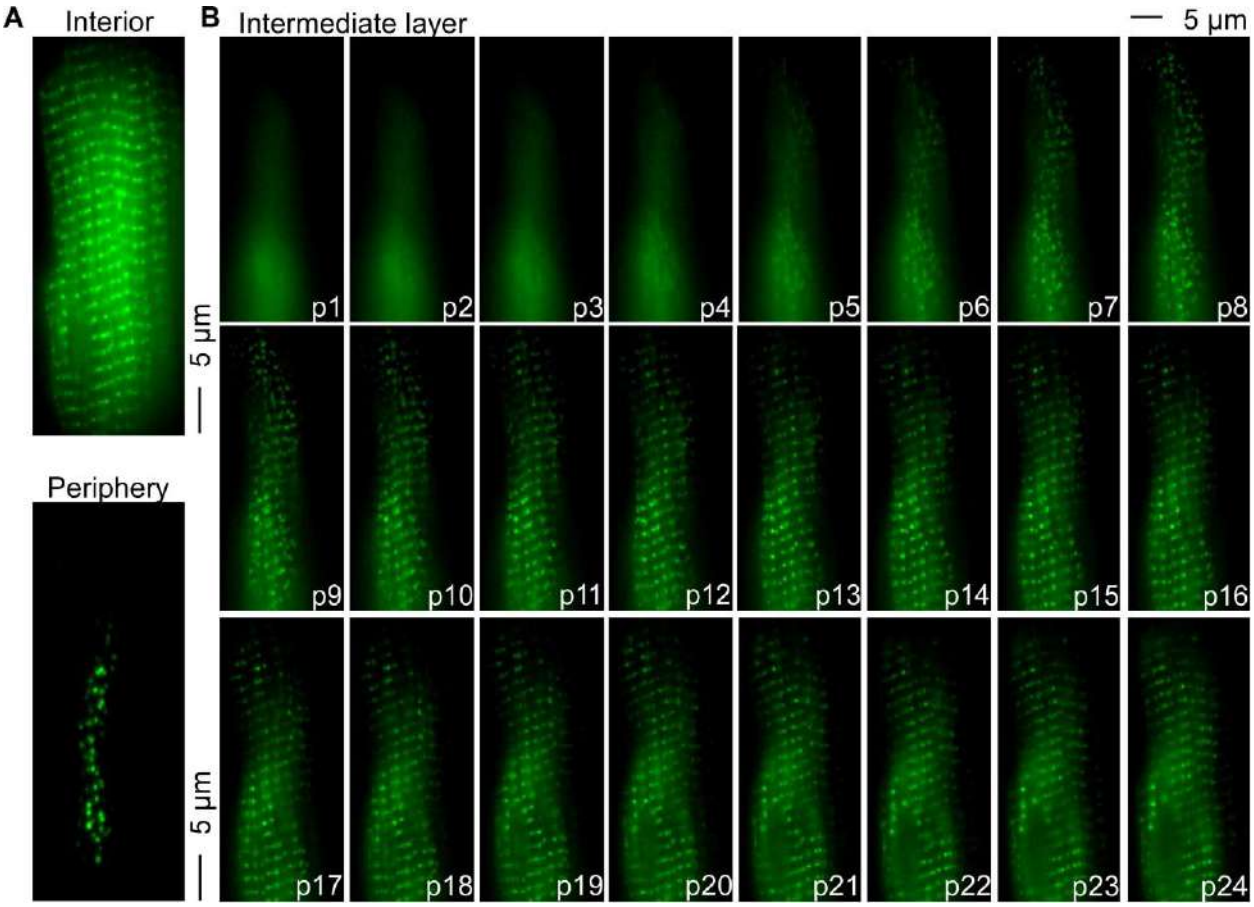

Supplemental Fig. 2. Imaging of Layers between the Interior and Periphery within the Same Ventricular Myocytes Detected using a TIRF Microscope

A. Representative images of periphery and interior in the same ventricular myocytes isolated from GFP-RyR2 mice were taken with a TIRF microscope. B, Optical z-stack planes (z stack distance 0.25um; plane *p1-24*) of layers with HILO illumination of the same cell. (n = 14 cells)

Supplemental Fig. 3

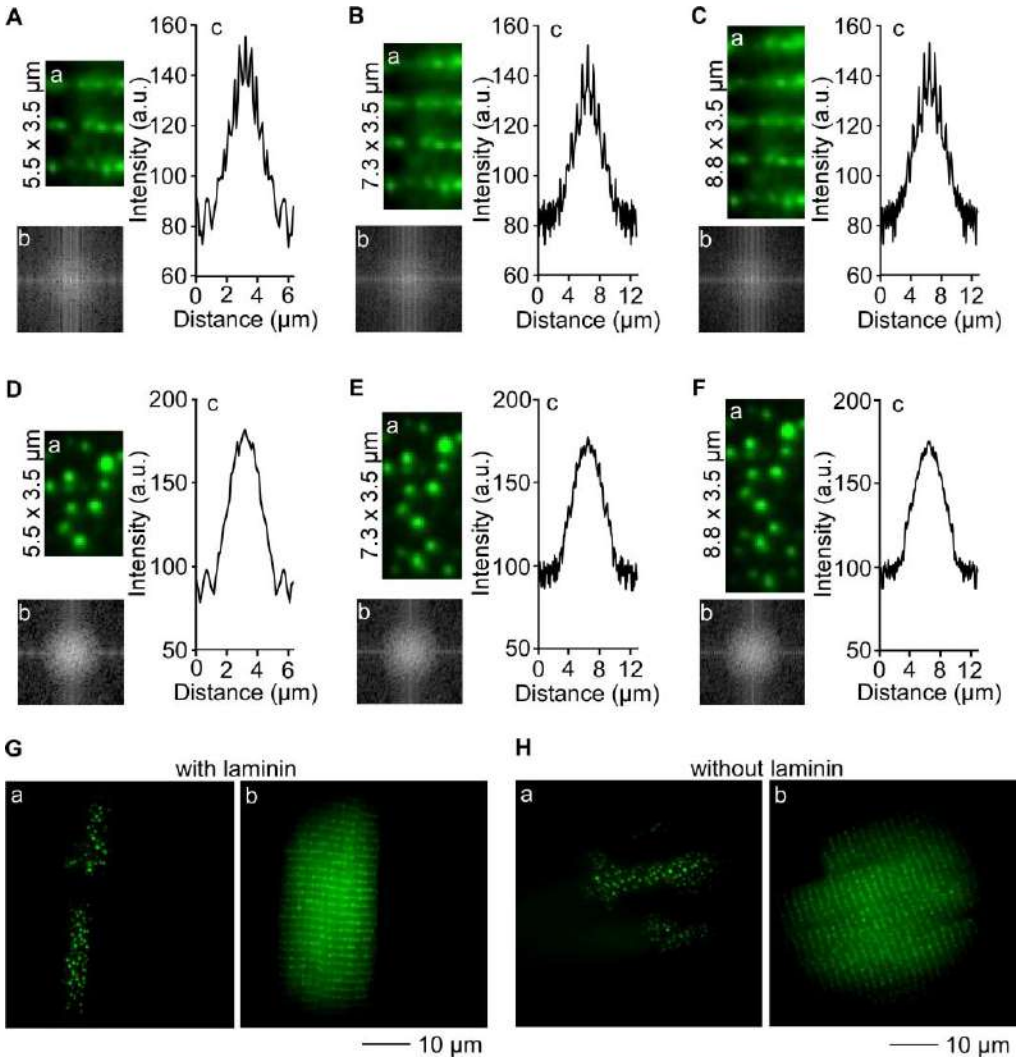

Supplemental Fig. 3. Fourier Transformation of Interior and Peripheral GFP-RyR2 Cluster Images with Different Area Sizes and Effects of Laminin on the Distribution of GFP-RyR2 Clusters in the Periphery and Interior of live Ventricular Myocytes

Fluorescence image areas with different sizes (A-F, panel a), corresponding 2D Fourier transforms (A-F, panel b), and intensity profiles derived from the Fourier transforms (A-F, panel c) of the interior (A-C) and the periphery (D-F) of live ventricular myocytes isolated from GFP-RyR2 mice are represented. Imaging of epi-fluorescent illuminated (angle = 0) interior showed highly-ordered, single-row arrays of GFP-RyR2 clusters (A-C, a). Irregular distribution of GFP-RyR2 clusters was found in the periphery through TIRF imaging (D-F, a). Distinct maxima were observed in all representative Fourier space of the interior (A-C, c), even in pattern analysis of areas as small as 5.5x3.5µm (A, c). In contrast, Fourier transform intensity profiles of the TIRF image of peripheral GFP-RyR2 clusters did not reveal intensity peaks in images with identical areas (D-F, c). Panels G and H shows TIRF images (a) and epi-fluorescence images (b) obtained from isolated GFP-RyR2 ventricular myocytes attached to glass coverslips with (G) and without (H) laminin coating.